

Response to Hot Deformation Conditions and Microstructure Development of Nimonic 80A Superalloy

DAVID BOMBAC¹, MIHAEL BROJAN², MILAN TERCELJ¹, AND RADO TURK¹

¹*Department of Materials and Metallurgy, Faculty of Natural Sciences and Engineering,
University of Ljubljana, Ljubljana, Slovenia*

²*Department of Mechanics, Faculty of Mechanical Engineering, University of Ljubljana,
Ljubljana, Slovenia*

Laboratory compression tests at different temperatures and strain rates have been performed on Nimonic 80A superalloy to define optimal hot forming characteristics. A mathematical expression connecting mean grain size and true stress is presented using a Hall–Petch-like equation. The evolution of microstructure at various sample positions in correlation with deformation temperatures, strain, and strain rates has also been investigated. Optimal hot-working conditions are determined using processing maps and obtained microstructure.

Keywords Activation energy; Compression tests; Dynamic material model; Dynamic recrystallization (DRX); Hall–Petch-like relationship; Hot deformation; Metallography; Nickel superalloy; Nimonic 80A; Optical microscopy; Precipitates; Processing maps; SAD pattern; TEM; Zener–Hollomon.

1. INTRODUCTION

Nimonic, a group of nickel-based superalloys, is a class of high temperature alloys intended for manufacturing and processing of sophisticated parts under heavy thermal stresses because of its specific material properties, e.g., high strength at elevated temperatures. The hot-working processing of such alloys is difficult due to its complex system of phases. The material response to hot deformation conditions is closely connected not only to the current values of the process parameters (equivalent strain, strain rate, and temperature) but also to precedent thermal and mechanical cycles.

The Nimonic 80A superalloy, contains Ti and Al, and has ordered γ' phase $\text{Ni}_3(\text{Al}, \text{Ti})$ along with primary carbides of general form MC as well as Cr rich grain-boundary carbides of type M_{23}C_6 . Carbides of type MC and M_{23}C_6 were found to precipitate from the matrix at temperatures between 760°C and 1000°C, while above 1000°C main carbides of type M_6C and less stable M_7C_3 will precipitate on grain boundaries where M is usually Cr, and less commonly W, Ta, Nb, [1–3]. Different thermomechanical treatment temperatures enable alteration of carbide type in the alloy. Best mechanical properties are obtained when homogenous fine grain microstructure is met. However, to predict the best hot processing parameters and final microstructure, a detailed understanding of the interactions between hot deformation behavior, softening mechanisms (recrystallization and recovery), and phase transformations is necessary, [4–6].

In this study laboratory compression tests at different temperatures and strain rates have been performed to define

the best hot-forming characteristics. The mean grain size and true stress relationship was determined using a Hall–Petch-like equation. The relationship of microstructure at various sample positions with deformation temperatures, strain, and strain rates has also been investigated with emphasis on dynamic recrystallization.

2. EXPERIMENTAL PROCEDURES

Hot workability of Nimonic 80A has been examined using a cylindrical compression test. The material was supplied by Metal Ravne, Slovenia, in the form of rods with diameter of 11 mm and chemical composition as presented in Table 1. The cylindrically shaped specimens ($\varnothing 10 \times 12$ mm) were machined from the supplied rod which has been rolled from a 90 mm square forged billet. Measured hardness of initial specimens was approximately 330 HB.

To determine hot-forming process parameters, physical simulations were carried out using a thermomechanical simulator, Gleeble 1500D. Simulation conditions were as follows: temperature range 950°C to 1120°C, and constant strain rates between 0.01 s^{-1} and 5.0 s^{-1} , cf. Table 2.

To avoid inhomogeneous deformation, Ta foils of 0.05 mm in thickness and graphite foils were inserted between the cylindrical specimen and the compression tool. The high-temperature microstructure was retained for light microscopy by water quenching just after the deformation to freeze the obtained microstructure. During the simulation experiments compression force, temperature of the specimen, shift of active jaws, change of specimen diameter, and time were measured and recorded. The stresses and strains for the evaluation of material flow curves and activation energies for hot deformation were calculated from the acquired data. Deformation heating temperature has been continuously monitored and regulated during deformation. Figure 1 shows a schematic time–temperature diagram of the hot compression process.

Received June 20, 2008; Accepted September 4, 2008

Address correspondence to David Bombac, Askerceva 12, SI-1000, Ljubljana, Slovenia; Fax: +386 1 4704 560; E-mail: david.bombac@ntf.uni-lj.si

TABLE 1.—Chemical composition of the Nimonic 80A alloy in wt%.

C	Si	Cu	Mn	Cr	Ti	Al	Fe	P	S	N ₂ ppm	O ₂ ppm
0.07	0.08	0.02	0.03	19.54	2.38	1.51	0.21	0.002	0.002	70	100

Deformed, water quenched samples were visually inspected, cut, and prepared for metallographic analysis. Details of microstructure were examined using conventional light microscopy and transmission electron microscopy (TEM) to identify carbides which appear in the alloy. The mean grain size was quantitatively determined by the image analysis using Olympus Analysis software.

3. RESULTS AND DISCUSSION

Typical single hit stress-strain curves (several tests were conducted for each set of conditions) are presented in this section. Figure 2 illustrates the effect of temperature on stress-strain curves determined at a strain rate of 0.1 s⁻¹. It can be seen that the flow stress values decrease with increasing temperature. Figure 3 depicts the effect of strain rate at a constant temperature of 1080°C on visco-elastic material behavior where the flow stress decreases with lower strain rates.

All flow curves displayed a rapid initial increase to a stress maximum, characterized by a peak stress and strain, followed by a decrease in flow stress to steady state. This behavior indicates that dynamic recrystallization occurs, cf. also [7]. A decrease of strain rate or a rise of temperature, with other parameters held constant, results in lower peak and lower steady stresses. This decrease can be due to lower effective stress to move dislocations and increased recrystallization.

TABLE 2.—Deformation conditions.

Strain	Strain rates [s ⁻¹]	Deformation Temperatures [°C]
1	0.01	950 1000 1040 1080 1120
1	0.1	950 1000 1040 1080 1120
1	1.0	950 1000 1040 1080 1120
1	5.0	950 1000 1040 1080 1120

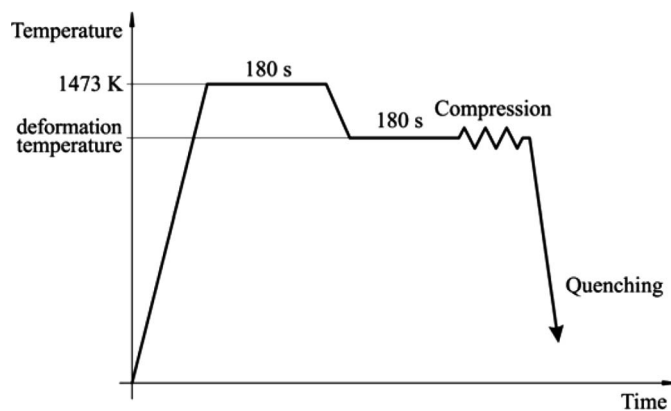


FIGURE 1.—Schematic diagram of the hot compression process.

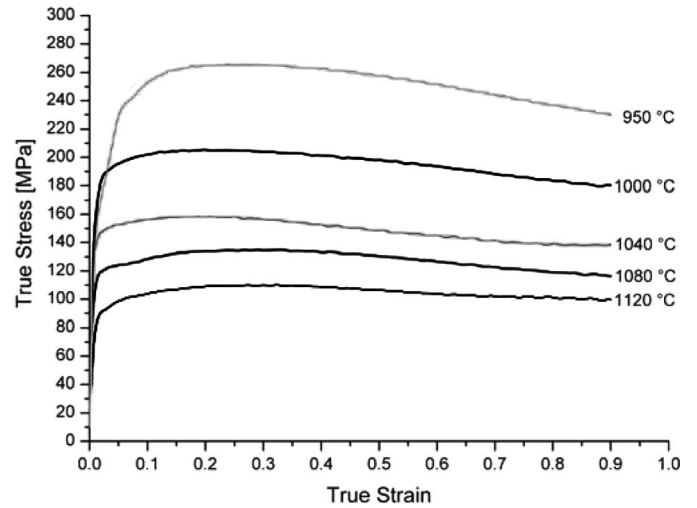


FIGURE 2.—Stress-strain curves in temperature range from 950°C to 1120°C at a strain rate of 0.1 s⁻¹.

Values for the peak stresses for all deformation conditions were collected and plotted in Fig. 4. There is a clear decaying trend of peak stress values when temperature is increased. As expected, peak stress values augment with increasing strain rate at any given temperature.

The activation energy for hot deformation can be derived using the following Zener-Hollomon parameter and hyperbolic sine equation:

$$Z = \dot{\epsilon} \exp\left(\frac{Q_{def}}{RT}\right) = A \sinh^n(\alpha\sigma). \tag{1}$$

Therefore,

$$Q_{def} = Rn \left[\frac{\partial \ln \sinh(\alpha\sigma)}{\partial \ln(T^{-1})} \right]_{\dot{\epsilon}=\text{const.}}, \tag{2}$$

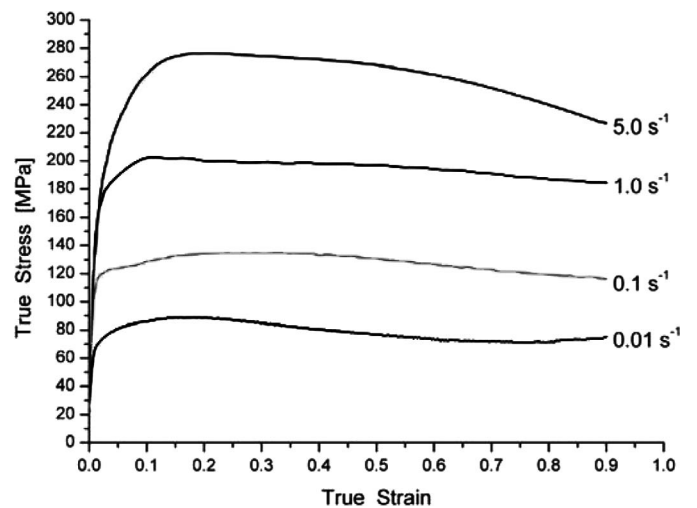


FIGURE 3.—Stress-strain curves at increasing strain rates at temperature of 1080°C.

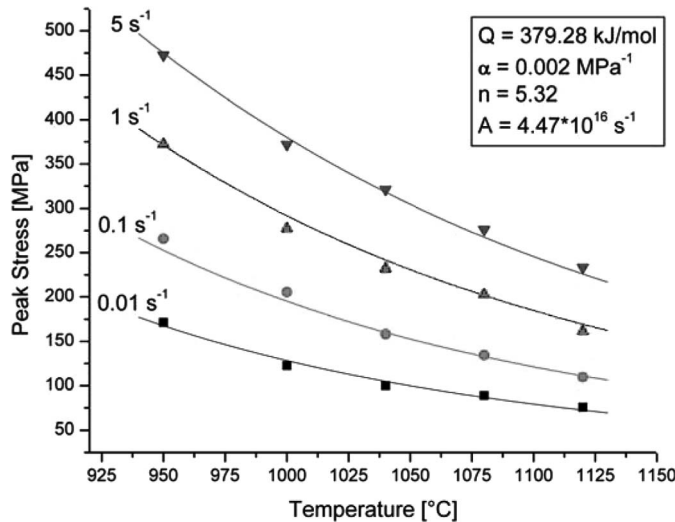


FIGURE 4.—Peak stress vs. temperature for different strain rates.

where Q_{def} is the activation energy for hot deformation determined from the peak stress and R is the gas constant. For this purpose the function χ^2 was defined first, which determines the difference between measured and calculated values of maximum flow stresses,

$$\chi^2 = \sum_{i=1}^N \frac{(z_i - a_1 x_i - a_2 y_i - a_3)^2}{e_i^2}, \quad (3)$$

where N is the number of measurements, $z_i = \ln(\sinh \alpha \sigma_i)$, $x_i = \ln \dot{\epsilon}_i$, and $y_i = 10^4 T^{-1}$. Parameter $a_1 = n^{-1}$, $a_2 = 10^{-4} Q n^{-1} R^{-1}$, and $a_3 = n^{-1} \ln A$. For the error calculation, we took into account only measurement errors of the parameter z_i , given by $e_i = \alpha e_i^\sigma \coth \alpha \sigma_i$, where e_i^σ are the measurement errors of the flow stress. The details of the minimization procedure of Eq. (3) are given elsewhere [8]. Application of Eq. (3) yields values of $\alpha = 0.002$, $n = 5.32$, and activation energy mean value of 379.28 kJ/mol.

The peak stress and temperature relation (see Fig. 4) can be described by a hyperbolic sine function, cf. Eq. (1). Good agreement between experimentally and analytically obtained results is also shown.

The relation between mean grain size and true stress was determined using a Hall–Petch-like relationship. A graphical presentation of experimental data and a fitted curve is presented in Fig. 5. The curve exhibits a typical power-law relation, with significantly increased true stress at lower mean grain diameter. The comparison of the true stress and mean grain size of the experimental results and that described by the Hall–Petch-like model shows good agreement.

Evolution of microstructure obtained with hot compression tests and optical microscopy is shown in Fig. 6. Micrographs in Fig. 6 have been taken from the center of the specimens. Initiation of dynamic recrystallization (DRX) on grain boundaries, which are preferential places for DRX initiation, [9] are also shown in Fig. 6. DRX start depends on temperature and strain rate and is shifted to lower

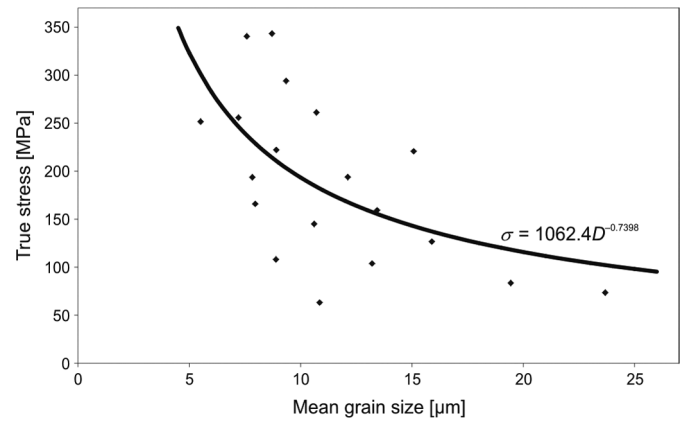


FIGURE 5.—Relation between mean grain size and steady state stress.

temperatures if the strain rate is lowered. The difference in microstructure development can be explained with inhomogeneous deformation and stress distribution. Critical deformation for DRX is first obtained at the center of the specimen, which was proved by microstructural examination and numerical simulation.

For the lowest strain rate of 0.01 s^{-1} dynamic recrystallization was observed for all temperatures investigated. However, the carbides rearrangement process did not occur at the lowest temperature of 950°C , but is clearly visible at higher temperatures. New recrystallized grains nucleate on grain boundaries of unrecrystallized grains and grow until driving energy for grain boundary movement is positive, or until contact with other growing DRX grains. As shown in Fig. 6, at middle temperatures and strain rates, the large unrecrystallized grains are surrounded by small grains, exhibiting a so called *necklace structure*. It can be concluded from the metallography that a fraction of recrystallized grains as a function of deformation temperature is higher when temperature is increased. Similar observations were derived when strain rate was lowered, which provides more time for DRX. These results comply with findings of other authors, cf. [3, 10]. Start of DRX with very small amount of recrystallized material volume is visible at highest strain rate (5 s^{-1}).

Microhardness measurements revealed a difference in microhardness of recrystallized grains, which varied between $270 \text{ HV}_{0.1}$ and $280 \text{ HV}_{0.1}$ and was lower than that for unrecrystallized grains, where it was between $310 \text{ HV}_{0.1}$ and $320 \text{ HV}_{0.1}$.

Precipitates can be identified using TEM bright field imaging. The method employed in the present work is similar to that in the literature, e.g., [10, 11]. In Nimonic 80A large TiC particles are usual. Carbides examined by TEM are arranged in two groups, as presented in Fig. 7. Identification of carbides was performed using selective area diffraction (SAD). In Figs. 7(b) and (d), SAD patterns of carbides are depicted.

Columnar shaped carbides presented in Fig. 7(a) were identified as metastable Cr_7C_3 , precipitated at grain boundaries. This carbide has a pseudo-hexagonal crystal structure and lattice parameter $a = 1.3980 \text{ nm}$ and $c = 0.4523 \text{ nm}$. Due to sample water quenching,

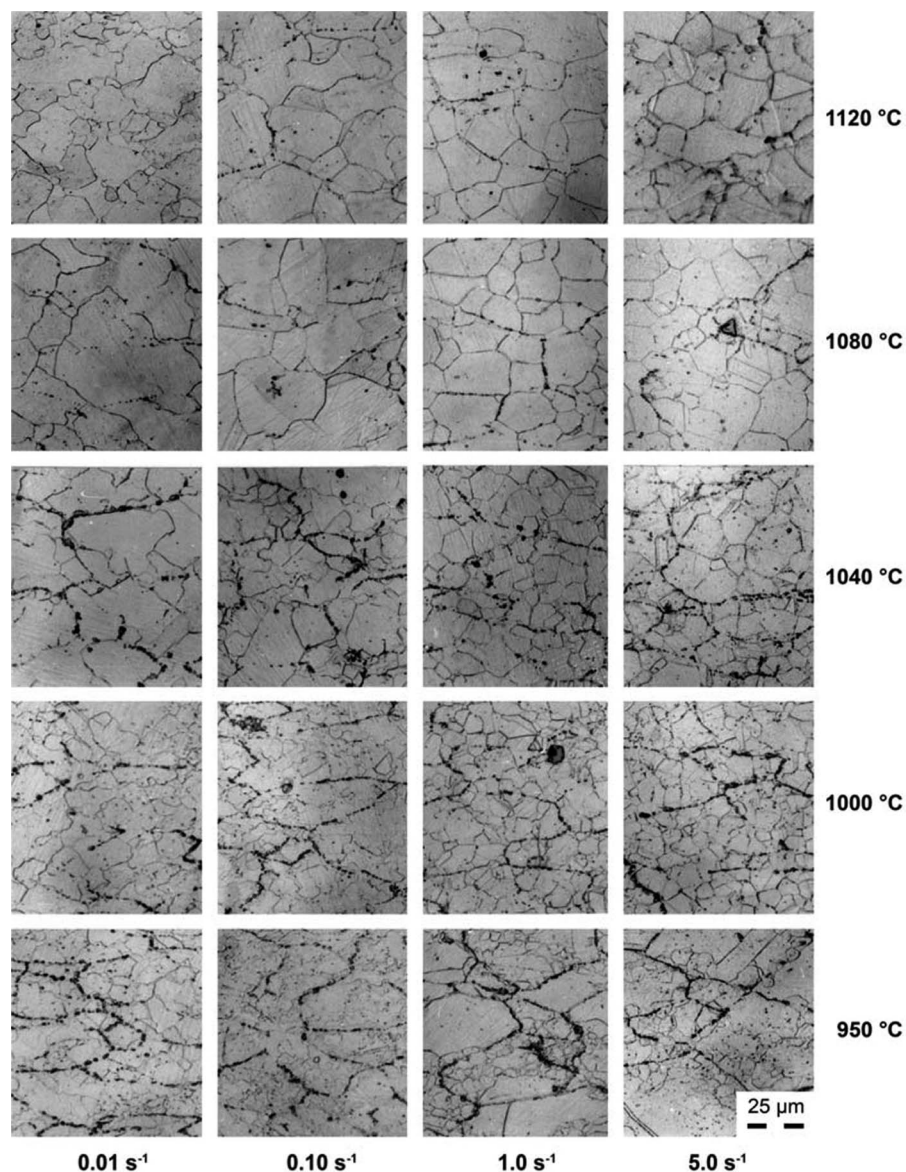


FIGURE 6.—Microstructure development dependent on the temperature and strain rate in the middle of the compression specimen.

metastable carbide Cr_7C_3 did not have enough time to form the stable Cr_{23}C_6 type. Spherically shaped carbides [Fig. 7(c)] were detected at grain boundaries and within grains. SAD identifies them as Cr_{23}C_6 . Precipitates within grains are significantly smaller than those found at grain boundaries.

Best hot-working conditions were established using processing maps of the Dynamic Material Model, see also [12]. Maps obtained at strains 0.1, 0.2, 0.3, and 0.6 are similar to each other, indicating the limited influence of strain. Processing maps revealed unstable regions at high temperatures and strain rates at strains 0.1 and 0.2. Nimonic 80A has a prominent high temperature domain with the peak efficiency of power dissipation being about 38%, where the corresponding strain rate is 0.1 s^{-1} between 1000°C and 1080°C .

4. CONCLUSION

From a practical standpoint, experimental results from this article can support the hot-forming process. The temperature region of plastic deformation is very important in achieving the best workability of desired metal alloys. Hot-forming processes such as forging or rolling are very important for industrial production. With correct reduction, especially at the end of the manufacturing process, homogeneously recrystallized fine-grain microstructure can be produced as was proved in our series of hot compression tests at various temperatures and strain rates. The following conclusions are drawn from the results of this article.

- 1) When strain rate is increased or temperature lowered, the apex of stress is shifted to higher strain.

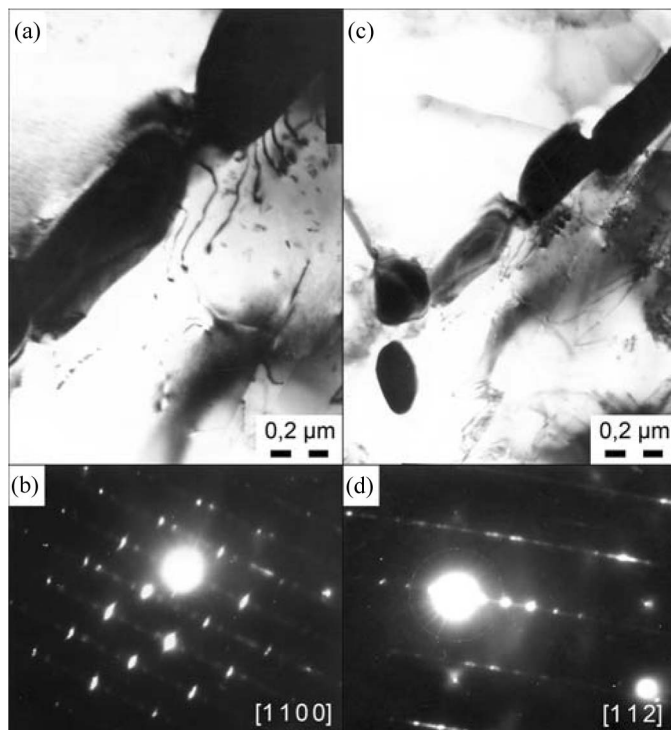


FIGURE 7.—TEM images of Nimonic 80A alloy, (a) columnar Cr_7C_3 carbide, (b) SAD pattern of Cr_7C_3 carbide, (c) spherical Cr_{23}C_6 carbide, and (d) SAD pattern of Cr_{23}C_6 carbide.

- 2) The fraction of recrystallized material is higher at increased temperatures and lowered strain rates. DRX starts at a strain rate 0.01 s^{-1} at 900°C .
- 3) Preferential carbides after hot deformation and water quenching are metastable columnar carbides Cr_7C_3 at grain boundaries. Small amounts of stable spherical carbides Cr_{23}C_6 precipitated at both grain boundaries and matrix.
- 4) The optimum hot working conditions lie between 1000°C and 1080°C , where corresponding peak efficiency is approximately 38%. Unstable regions were found at strains of 0.1 and 0.2 at high temperatures and strain rates.

REFERENCES

1. Wilthan, B.; Tanzer, R.; Schützenhöfer, W.; Pottlacher, G. Thermophysical properties of the Ni-based alloy Nimonic 80A up to 2400 K, III. *Thermochimica Acta* **2007**, *465* (1–2), 83–87.
2. Bariani, P.F.; Bruschi, S.; Dal Negro, T. Prediction of nickel-base superalloys' rheological behaviour under hot forging conditions using artificial neural networks. *Journal of Materials Processing Technology* **2004**, *152* (3), 395–400.
3. Srinivasa, N.; Prasad, Y.V.R.K. Hot working characteristics of nimonic 75, 80A and 90 superalloys: A comparison using processing maps. *Journal of Materials Processing Technology* **1995**, *51* (1–4), 171–192.
4. Sakai, T.; Ohashi, M.; China, K.; Jonas, J.J. Recovery and recrystallization of polycrystalline nickel after hot working. *Acta Metallurgica* **1988**, *36* (7), 1781–1790.
5. Whillock, R.T.J.; Buckley, R.A.; Sellars, C.M. The influence of thermomechanical processing on recrystallization and precipitation in austenitic alloys with particular reference to the effects of deformation and ageing conditions. *Materials Science and Engineering A* **2000**, *276* (1–2), 124–132.
6. Myshlyayev, M.M.; McQueen, H.J.; Mwembela, A.; Konopleva, E. Twinning, dynamic recovery and recrystallization in hot worked Mg–Al–Zn alloy. *Materials Science and Engineering A* **2002**, *337* (1–2), 121–133.
7. Roucoules, C.; Yue, S.; Jonas, J.J. Effect of alloying elements on metadynamic recrystallization in HSLA steels. *Metallurgical and Materials Transactions A* **1995**, *26* (1), 181–190.
8. Kugler, G.; Knap, M.; Palkowski, H.; Turk, R. Estimation of activation energy for calculating the hot workability properties of metals. *Metalurgija* **2004**, *43* (4), 267–272.
9. Kugler, G.; Turk, R. Modeling the dynamic recrystallization under multi-stage hot deformation. *Acta Materialia* **2004**, *52* (15), 4659–4668.
10. Tian, B.; Lind, C.; Paris, O. Influence of Cr_{23}C_6 carbides on dynamic recrystallization in hot deformed Nimonic 80a alloys. *Materials Science and Engineering A* **2003**, *358* (1–2), 44–51.
11. Tian, B.; Zickler, G.A.; Lind, C.; Paris, O. Local microstructure and its influence on precipitation behavior in hot deformed Nimonic 80a. *Acta Materialia* **2003**, *51* (15), 4149–4160.
12. Prasad, Y.V.R.K.; Sasidhara, S. *Hot Working Guide: A Compendium of Processing Maps*; ASM International: Materials Park, Ohio, 1997; 545 pp.